Development of a unique 3D interaction model of endogenous and synthetic peripheral benzodiazepine receptor ligands

Nunzia Cinone[a,*], Hans-Dieter Höltje[b] & Angelo Carotti[a,**]

[a]*Dipartimento Farmaco Chimico, Università degli Studi di Bari, via E. Orabona 4, I-70125 Bari, Italy;* [b]*Institute of Pharmaceutical Chemistry, Heinrich-Heine-University Düsseldorf, Universitätsstrasse 1, D-40225 Düsseldorf, Germany*

Summary

Different classes of Peripheral-type Benzodiazepine Receptor (PBR) ligands were examined and common structural elements were detected and used to develop a rational binding model based on energetically allowed ligand conformations. Two lipophilic regions and one electrostatic interaction site are essential features for high affinity ligand binding, while a further lipophilic region plays an important modulator role. A comparative molecular field analysis, performed over 130 PBR ligands by means of the GRID/GOLPE methodology, led to a PLS model with both high fitting and predictive values ($r^2 = 0.898$, $Q^2 = 0.761$). The outcome from the 3D QSAR model and the GRID interaction fields computed on the putative endogenous PBR ligands DBI (Diazepam Binding Inhibitor) and TTN (Tetracontatetraneuropeptide) was used to identify the amino acids most probably involved in PBR binding. Three amino acids, bearing lipophilic side chains, were detected in DBI (Phe49, Leu47 and Met46) and in TTN (Phe33, Leu31 and Met30) as likely residues underlying receptor binding. Moreover, a qualitative comparison of the molecular electrostatic potentials of DBI, TTN and selected synthetic ligands indicated also similar electronic properties. Convergent results from the modeling studies of synthetic and endogenous ligands suggest a common binding mode to PBRs. This may help the rational design of new high affinity PBR ligands.

Introduction

Peripheral-type Benzodiazepine (BZ) Receptors (PBRs) have been identified in various peripheral tissues [1] as well as in glial cells in the Central Nervous System (CNS), where the BZ binding GABA$_A$ receptors are also abundant. PBRs are located mainly on the outer mitochondrial membrane and bind with high affinity the BZ derivative Ro5-4864 and the isoquinoline carboxamide derivative PK11195 [2, 3] (Chart 1). Many other BZs elicit very low binding affinity toward PBRs [4].
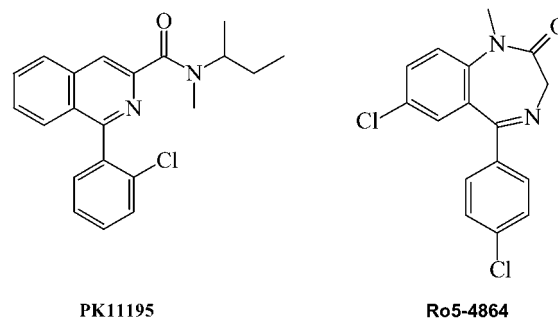

PK11195   **Ro5-4864**

Chart 1. Structures of PK11195 and R05-4864.

PBRs and GABA$_A$ receptors are indeed distinct proteins differing in terms of tissue distribution, subcellular localization and pharmacological profile [5]. Nevertheless, they share a common role in the CNS

where both modulate the GABA-ergic transmission. Growing evidence suggests that PBRs are involved in several functions such as cell proliferation, immune response modulation, regulation of mitochondrial oxidative phosphorylation and, most importantly, of steroidogenesis [5–8]. As for the latter, PBRs promote the cholesterol influx from the outer to the inner mitochondrial membrane where it is converted into pregnenolone by cytochrome P450 scc (side chain cleavage). Moreover, recent findings pointed out an overexpression of PBRs in brain tumors, suggesting also a possible use of PBR ligands as imaging agents or as specific carriers of antitumor drug carriers [9–11]. In spite of these recent significant advances, the physiological role of PBRs has not been fully defined yet.

In this scenario, in order to better characterize the potential pharmacological and therapeutic roles of PBRs, several studies have been addressed at the preparation of new PBR ligands displaying both high binding affinity and selectivity towards PBRs [4, 12–21]. Actually, the rational design of such ligands is strongly hampered by the lack of precise information, at the structural and molecular level, on the PBR putative binding sites of synthetic and endogenous ligands.

From a structural point of view, PBRs are formed by distinct protein subunits of 30, 32 and 18 kDa, that represent the Adenine Nucleotide Carrier (ANC), the Voltage Operated Anion Channel (VOAC) and the isoquinoline carboxamide binding protein, respectively [2, 3]. The latter interacts both with PK11195 and Ro5-4864, but with different and only partially overlapped binding sites [22, 23]. Other studies have been focused on the discovery and characterization of possible endogenous ligands of PBRs. Most of them are consistent with the hypothesis that the Diazepam Binding Inhibitor (DBI [24]) and some shorter peptides, deriving from its proteolytic degradation, may be the natural endogenous modulators of both PBR (directly) and GABA$_A$ receptors (indirectly, by influencing the neurosteroidogenesis [24–26]).

In the absence of any reliable direct structural investigation on PBRs, some indirect (ligand-based) approaches have been applied to some classes of PBR ligands to gain insight into the key molecular determinants of high receptor affinity.

So far, Structure Activity Relationship (SAR [4, 12–22, 27–30]) and three-dimensional Quantitative Structure-Activity Relationship (3D QSAR [31]) studies have been conducted only on congeneric series of

PBR ligands and therefore the generation of a comprehensive model based on a higher number of ligands showing a greater molecular diversity could be an important objective for medicinal chemists. Moreover, useful information capable also to validate the results from the 3D QSAR studies, could be derived through the modeling of the putative endogenous PBR ligands and a subsequent comparison, at the three-dimensional level, of their steric, electronic and lipophilic properties with those shared by high affinity synthetic ligands of PBR. Following this reasoning a modeling study on synthetic and endogenous PBR ligands was carried out to reach several important goals: (i) the development of a general, statistically robust 3D QSAR model for structurally diverse PBR ligands; (ii) the identification of the crucial amino acids of endogenous ligands most likely involved in the ligand binding with PBR; (iii) the identification of a possible common binding mode for synthetic and endogenous ligands of PBRs.

Material and methods

Biological data and selection of ligands

The compounds investigated in this study belong to approximately three different classes of PBR ligands, which are structurally unrelated: (I) pyrrolobenzothiazepine [15, 27–28, 30] and pyrrolobenzoxazepine [29] derivatives, (II) quinoline and isoquinoline derivatives [20], (III) pyrrolopyridin-5-one and pyrroloquinolin-1-one derivatives [14]. These compounds are listed in Tables 1a,b, 2 and 3 along with their biological data.

The binding data represent the ligand ability to displace the isoquinoline carboxamide derivative [^{3}H]PK11195 from its PBR binding site in rat cortex homogenate and are expressed as pIC$_{50}$. Since PK11195 is the common reference compound in all the biological assays, its IC$_{50}$ value was used to normalize the data from different laboratories. IC$_{50}$ of PK11195 fluctuates around the value of 2 nM in all the assays, since they were performed under the same experimental conditions. Several binding affinities listed in Tables 1, 2 and 3 are not accurately defined since they refer to nearly inactive compounds for which the IC$_{50}$ values are higher than 10 000 nM. To avoid the loss of relevant information for our QSAR studies, these compounds were included in our investigations with truncated affinity values (pIC$_{50}$ = 4.0).

In view of the homogeneity, good spread (over five orders of magnitude) and distribution of the biolog-

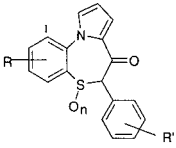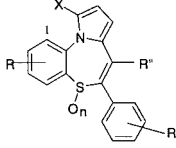*Table 1a.* Chemical structures and biological data of pyrrolo[2,1-d][1,5]benzothiazepine derivatives **1–67**

Compd.	R	R′	n	R″	X	pIC$_{50}$[a]
1	H	H	0		H	5.91
2	H	4-OCH$_3$	0		H	5.68
3	2-CF$_3$	4-OCH$_3$	0		H	5.21
4	2-Cl	4-OCH$_3$	0		H	5.85
5	H	H	1		H	4.83
6	H	H	2		H	4.00
7	H	4-OCH$_3$	1		H	4.64
8	H	H	0	OSO$_2$CH$_3$	H	7.22
9	H	H	0	OCOCH$_3$	H	7.70
10	H	H	0	OCOC$_2$H$_5$	H	7.17
11	H	H	0	OCO-n-C$_3$H$_7$	H	7.66
12	H	H	0	OCO-n-C$_4$H$_9$	H	7.32
13	H	H	0	OCO-n-C$_5$H$_{11}$	H	7.64
14	H	H	0	OCON(CH$_3$)$_2$	H	8.04
15[b]	H	H	0	OCON(CH$_3$)$_2$	H	5.87
16	H	4-OCH$_3$	0	OCO-n-C$_3$H$_7$	H	7.55
17	2-CF$_3$	4-OCH$_3$	0	OCOCH$_3$	H	4.00
18	2-CF$_3$	4-OCH$_3$	0	OCOC$_2$H$_5$	H	5.53
19	2-CF$_3$	4-OCH$_3$	0	OCON(CH$_3$)$_2$	H	6.54
20	2-CF$_3$	4-OCH$_3$	0	OCOC$_6$H$_2$-3,4,5(OCH$_3$)$_3$	H	4.00
21	2-Cl	H	0	OCOCH$_3$	H	6.25
22	2-Cl	H	0	OCOC$_2$H$_5$	H	6.09
23	2-Cl	4-OCH$_3$	0	OCOCH$_3$	H	6.19
24	2-Cl	4-OCH$_3$	0	OCOC$_2$H$_5$	H	6.31
25	2-Cl	4-OCH$_3$	0	OCON(CH$_3$)$_2$	H	6.77
26	2-Cl	4-OCH$_3$	0	OCOC$_6$H$_2$-3,4,5(OCH$_3$)$_3$	H	4.00
27	3-Cl	H	0	OCOCH$_3$	H	6.64
28	3-Cl	4-OCH$_3$	0	OCOCH$_3$	H	6.62
29	4-Cl	H	0	OCOCH$_3$	H	8.10
30	4-Cl	4-OCH$_3$	0	OCOCH$_3$	H	7.70
31	2-OCH$_3$	4-OCH$_3$	0	OCOCH$_3$	H	5.74
32	H	H	1	OCOCH$_3$	H	6.16
33	H	H	2	OCOCH$_3$	H	5.94
34	H	4-OCH$_3$	1	OCOCH$_3$	H	5.68
35	H	4-OCH$_3$	2	OCOCH$_3$	H	6.19
36	H	4-OCH$_3$	1	OCOC$_3$H$_7$	H	6.57
37	H	4-OCH$_3$	0	OCON(CH$_3$)$_2$	H	8.04
38	H	4-OCH$_3$	0	OCOCH$_3$	H	7.47
39	H	4-OCH$_3$	0	OSO$_2$CH$_3$	H	7.02
40	H	4-OCH$_3$	0	OCO-3-pyridyl	H	4.00
41	H	4-OCH$_3$	0	OCOC$_6$H$_2$-3,4,5(OCH3)$_3$	H	4.00
42	H	4-OCH$_3$	0	OCOC$_2$H$_5$	H	7.52
43	H	4-OCH$_3$	0	OCO-4-pyridyl	H	4.00
44	H	2-F	0	OCOCH$_3$	H	7.42

Table 1a (continued).

Compd.	R	R'	n	R''	X	pIC$_{50}$[a]
45	H	2-F	0	OCON(CH$_3$)$_2$	H	7.51
46	H	4-Cl	0	OCOCH$_3$	H	7.52
47	H	4-F	0	OCOCH$_3$	H	7.55
48	2-CH$_3$	H	0	OCOCH$_3$	H	6.17
49	3-CH$_3$	H	0	OCOCH$_3$	H	6.95
50	4-Cl	H	0	OCON(CH$_3$)$_2$	H	8.40
51	H	H	0	OCON(C$_2$H$_5$)$_2$	H	8.33
52	H	H	0	OCO(CH$_2$)$_5$CH$_3$	H	8.25
53	H	H	0	OCO(CH$_2$)$_6$CH$_3$	H	7.26
54	H	H	0	OCOC$_6$H$_{11}$	H	6.42
55	1-CH$_3$	H	0	OCOCH$_3$	H	5.30
56	1-CH$_3$	H	0	OCON(CH$_3$)$_2$	H	5.62
57	1-Cl	H	0	OCON(CH$_3$)$_2$	H	5.30
58	4-Cl	H	0	OCON(C$_2$H$_5$)$_2$	H	8.70
59	H	4-Cl	0	OCON(iC$_3$H$_7$)$_2$	H	7.96
60	H	4-Cl	0	OCON(CH$_2$CH$_2$)$_2$O	H	8.41
61	H	H	0	H	H	5.50
62	H	H	0	OCH$_3$	H	5.15
63	1-Cl	H	0	OCOCH$_3$	H	4.00
64	H	H	0	OCOCH$_3$	O	4.00
65	2-Cl	4-OCH$_3$	0	OCOCH$_3$	CH$_2$-N(CH$_3$)$_2$	5.70
66	2-Cl	H	0	OCOCH$_3$	CH$_2$-N(CH$_3$)$_2$	5.70
67	H	H	0	OCOCH$_3$	CH$_2$-N(CH$_3$)$_2$	5.70

[a]Data for compounds **1–14**, **16–50**; **15**, **51–60**, **63–64**; **61–62**; **65–67** are from References 27, 28, 30, 15, respectively.
[b]4-[(Dimethylcarbamoyl)oxy]-5-phenyl-11H-pyrrolo[2,1-d]-[1,5]benzothiazocine.

ical data, these compounds represent a suitable set for developing 3D QSARs by means of a comparative molecular field analysis approach [32].
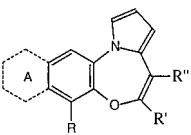
Molecular modeling

Synthetic compounds. The molecular structures of the examined ligands were constructed on the basis of the X-ray crystallographic data available for compounds **14**, **25**, **38**, **39** and **45** from CSD [33] (entry: ZILSUI, ZILTOD, ZILTET, ZILTIX, ZILTAP respectively) or by using the fragment library of the molecular modeling program SYBYL 6.5 [34] (Tripos Associates Inc., St. Louis, MO, U.S.A.). Geometry optimization was carried out by molecular mechanics by means of the TRIPOS force field [35] (conjugate gradient algorithm; iteration:1000; convergence criterion: 0.001 kcal/molÅ). In addition the vdW radius of the hydrogen atom was set to 1.2 Å. The conformational analysis was performed by using the Random Search option of SYBYL. This tool yields energetically allowed conformations by randomly modifying torsions, minimizing and eliminating duplicates so that the huge number of theoretical conformers is drastically reduced. The minimization was reached applying the conjugate gradient algorithm and employing a convergence criterion of 0.05 kcal/molÅ.

A literature survey revealed that several SAR [4, 12–22, 27–30] studies have been performed separately on congeneric classes of PBR ligands. The evident similarity between the topological and electronic features among the examined classes of PBR ligands suggests the tempting hypothesis that a comprehensive interaction model for all the PBR ligands is conceivable. Figure 1 shows a plausible interaction model for the three main classes (I, II, III) of PBR ligands. It consists of three lipophilic regions (L1, L3 and L4), and an electron rich zone close to the carbonyl oxygen (H2).

The L4 region probably plays a modulator role in the ligand binding to PBR. This is supported by the observation that the 7-OCON(C$_2$H$_5$)$_2$ pyrrolobenzothiazepine and pyrrolobenzoxazepine derivatives

Table 1b. Chemical structure and biological data of pyrrolo[2,1-d][1,5] benzoxazepine derivatives **68**-**86**

| Compd.	A	R	R$'$	R$''$	pIC$_{50}$[a]
68	none	H	C$_2$H$_5$	OCOCH$_3$	5.30
69	none	H	C$_2$H$_5$	OCON(CH$_3$)$_2$	8.23
70	none	H	C$_6$H$_5$	OCOCH$_3$	7.92
71	none	H	C$_6$H$_5$	OCOC$_6$H$_{11}$	7.09
72	none	H	C$_6$H$_5$	OCON(CH$_3$)$_2$	8.29
73	none	H	C$_6$H$_5$	OCON(C$_2$H$_5$)$_2$	9.17
74	none	H	C$_6$H$_5$	OCSN(C$_2$H$_5$)$_2$	8.42
75	none	H	C$_6$H$_4$-pCH$_3$	OCOCH$_3$	8.64
76	none	H	C$_6$H$_4$-pCH$_3$	OCON(CH$_3$)$_2$	8.89
77	none	H	C$_6$H$_4$-pCH$_3$	OCON(C$_2$H$_5$)$_2$	9.03
78	none	H	2-naphthyl	OCOCH$_3$	7.11
79	none	H	2-naphthyl	OCON(CH$_3$)$_2$	8.22
80	none	H	C$_6$H$_4$-pN$_3$	OCON(CH$_3$)$_2$	8.44
81	none	Cl	C$_6$H$_5$	OCON(CH$_3$)$_2$	8.89
82	benzo	H	C$_6$H$_5$	OCOCH$_3$	6.55
83	benzo	H	C$_6$H$_5$	OCON(CH$_3$)$_2$	7.43
84	none	H	C$_6$H$_5$	COOCH$_3$	6.83
85	none	H	C$_6$H$_5$	COCH$_3$	7.19
86	none	H	C$_6$H$_5$	CH$_2$OCOCH$_3$	5.71

[a]Data from Reference 29.
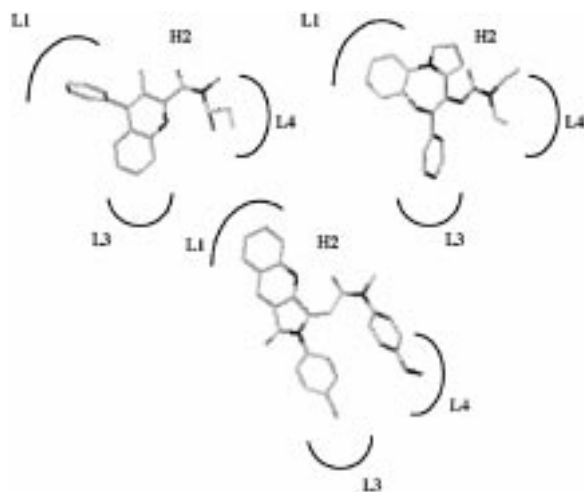
Figure 1. Representation of the integrated interaction model at PBR; the most active compounds of classes I, II and III are shown as reference compounds: **101**, pIC$_{50}$ = 8.77 (upper left); **73**, pIC$_{50}$ = 9.17 (upper right); **121**, pIC$_{50}$ = 8.72 (lower). L1, L3 and L4 correspond to three lipophilic regions; H2 corresponds to an electron rich zone.

have greater affinity then the corresponding 7-OCON(CH$_3$)$_2$ derivatives (**77** vs **76**, **57** vs **49** and **50** vs **14**).

All the ligands belonging to classes I, II and III were aligned following the principles of the Active Analog Approach [36], which uses the most rigid and potent derivative as the template to restrict the ligand conformational space only to regions accessible to active and rigid ligands. Since we excluded from our investigations the relatively rigid Ro5-4864, because, as already anticipated, it may have a specific binding site only partially overlapping with that of isoquinoline carboxamide PK11195, we had to overcome first the problem of the lack of a rigid compound in our set of ligands. The most crucial step for the ligands overlay was therefore the selection of the conformation of freely rotating side chains which carry the carbonyl groups. Compound **101** was chosen as the template because of its high affinity and relatively low flexibility. Assuming the two aromatic rings and the electron rich group to be the anchor points in the interaction model,

Table 2. Chemical structure and biological data of quinolines and isoquinolines derivatives **87**–**116** (General Structures A–E)
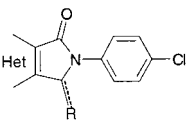

Compd.	G.S.	Bridge (Y)	R	X	R'	R''	pIC_{50}[a]
87	A	CH_2		H	s-C_4H_9		5.00
88	A	CH_2		F	s-C_4H_9		5.00
89	A	CH_2		H	CH_2-C_6H_5		5.00
90	A	CH-nC_4H_9		H	CH_2-C_6H_5		6.09
91	A	$CH_2CH_2CH_2$		H	CH_3		5.00
92	A	$CH_2CH_2CH_2$		H	s-C_4H_9		5.92
93	A	$CH_2CH_2CH_2$		H	CH_2-C_6H_5		6.77
94	B			H	s-C_4H_9	H	6.64
95	B			F	s-C_4H_9	H	7.89
96	B			H	CH_2-C_6H_5	H	5.92
97	B			H	CH_2-C_6H_4-4Cl	H	5.77
98	B			F	CH_2-C_6H_4-4Cl	H	6.57
99	B			H	s-C_4H_9	CH_3	8.77
100	B			F	s- C_4H_9	CH_3	8.54
101	B			H	CH_2-C_6H_5	CH_3	8.77
102	B			H	CH_2-C_6H_4-4Cl	CH_3	8.01
103	B			F	CH_2-C_6H_4-4Cl	CH_3	8.47
104	B			H	C_6H_4-4Cl	CH_3	8.19
105	B			H	C_6H_4-4OCH_3	CH_3	8.05
106	C	CH_2			s-C_4H_9		6.21
107	C	CH_2			CH_2-C_6H_5		6.32
108	C	$CH_2CH_2CH_2$			s-C_4H_9		6.11
109	C	CH=CHCH_2			s-C_4H_9		6.31
110	C	CH=CHCH_2			CH_2-C_6H_5		7.35
111	D	CH_2CH_2					8.05
112	D	OCH_2CH_2					8.00
113	E		H	Cl	s-C_4H_9	CH_3	8.70
114	E		CH_3	H	s-C_4H_9	H	6.26
115	E		CH_3	H	s-C_4H_9	CH_3	7.96
116	E		CH_3	H	CH_2-C_6H_5	CH_3	8.51

[a]Data from Reference 20.

Table 3. Chemical structure and biological data of pyrrolopyridin-5-one and pyrroloquinolin-1-one derivatives **117-130**

Compd.	Het[b]	Conf.[c]	R	R$'$	R$''$	pIC$_{50}$[a]
117	Q	Z	CHCONR$'$R$''$	n-C$_3$H$_7$	n-C$_3$H$_7$	7.40
118	Q	Z	CHCONR$'$R$''$	n-C$_6$H$_{11}$	n-C$_6$H$_{11}$	6.82
119	Q	Z	CHCONR$'$R$''$	CH$_3$	CH$_2$-C$_6$H$_5$	6.00
120	Q	Z	CHCONR$'$R$''$	C$_2$H$_5$	CH$_2$-C$_6$H$_5$	6.00
121	Q	Z	CHCONR$'$R$''$	CH$_3$	C$_6$H$_4$-4OCH$_3$	8.72
122	Q	Z	CHCONR$'$R$''$	CH$_3$	C$_6$H$_4$-4Cl	7.49
123	Q		CH$_2$CONR$'$R$''$	n-C$_3$H$_7$	n-C$_3$H$_7$	6.00
124	Q		CH$_2$CONR$'$R$''$	n-C$_6$H$_{11}$	n-C$_6$H$_{11}$	6.00
125	P	Z	CHCONR$'$R$''$	n-C$_3$H$_7$	n-C$_3$H$_7$	6.54
126	P	Z	CHCONR$'$R$''$	n-C$_6$H$_{11}$	n-C$_6$H$_{11}$	4.48
127	P		CH$_2$CONR$'$R$''$	n-C$_3$H$_7$	n-C$_3$H$_7$	6.00
128	P		CH$_2$CONR$'$R$''$	n-C$_6$H$_{11}$	n-C$_6$H$_{11}$	5.79
129	Q	E	CHCONR$'$R$''$	n-C$_3$H$_7$	n-C$_3$H$_7$	6.00
130	P		H$_2$			6.00

[a]Data **117–130** are from Reference 14.
[b]Q and P stand for [b]-fused quinoline or pyridine, respectively.
[c]Configuration of C=R double bond.

three dummy atoms were constructed and used for the superimposition: two centroids for the aromatic rings (L1, L3) and one lone pair of the carbonyl group (distal lone pair to L1), since it showed more consistent overlay in terms of fitting and directionality.

In the template compound **101**, there exists more than one conformational constraint driving the ligand into a favourable conformation. In fact, in this compound the steric repulsion between the N-methyl group and the methyl substituent on the quinoline ring makes a large portion of the conformational space energetically inaccessible. Moreover, the phenyl ring substituent of the amide nitrogen atom could be involved in a π-π interaction with the quinoline ring. All that may induce the template to assume a favourite conformation with a dihedral angle between the plane of the bicyclic aromatic system and the carbonyl plane around 50°.

Endogenous ligands. The DBI (86aas) is the putative precursor of a number of physiological allosteric modulators of GABA$_A$ and PBR receptors, through which it controls the rate limiting step of the steroidogenesis, that is the cholesterol influx into mitochondria [7, 24,

25] (Table 4). DBI was independently purified [37] and characterized for its ability to bind to long chain acyl-CoA esters and modulate the lipid metabolism [38].

The three-dimensional structure of DBI was built from the coordinates of 29 conformers detected by NMR spectroscopy [39] and recovered from the Protein Brookhaven Database (PDB, entry 2ABD). The structure consists of four α-helices: A1 (residues 3 to 15), A2 (residues 20 to 36), A3 (residues 51 to 60) and A4 (residues 65 to 85). A1 and A4 as well as A2 and A3 run in a parallel way.

Unlike the compounds resolved by X-ray crystallography, which are deposited in the PDB as a single structure, each NMR derived structure is often deposited as an ensemble of many conformers. To select a single 'representative' structure or a 'representative' subset of structures from such an ensemble, we used a computer program, called NMRCLUST [40], which clusters the structures into a set of conformationally related subfamilies. The method of average linkage was used to build up the clusters, followed by the application of a penalty function to simultaneously minimize the number of clusters and the spread

Table 4. Binding data of DBI and other native peptide fragments[a]

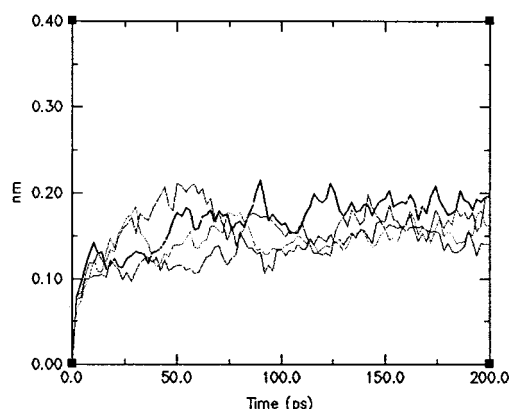| Peptides	^{3}H-Flumazenil binding to cerebellar granule cells (Ki, μM)	^{3}H-PK11195 binding to astrocyte mitochondria (Ki, μM)
DBI (1–86)	5	5
ODN (33–50)	5	>100
TTN (17–50)	>100	10

[a]Data from Reference 25.

Figure 2. RMSD of all the DBI backbone atoms from the NMR-derived structures for the five representative structures (see text).

Table 5. Binding of DBI processing products[a]

Peptides	IC$_{50}$ [^{3}H]Ro5-4864 binding to astrocytes membranes (μM)
TTN (17–50)	6
(22–50)	7
EPN (26–50)	>50
(19–41)	>50
ODN (33–50)	>50

[a]Data from Reference 26.

across each cluster. To perform such a cluster analysis NMRCLUST derives a distance matrix by superposing each atom of one of the members of the ensemble onto the corresponding atom of the other members in a pairwise manner. The set of atoms on which the superposition was carried out, was selected by using the software NMRCORE [41]. This is an automatic method that determines the optimum set of atoms, called Local Structure Domain (LSD), to be used for superposition, by analysing the variance of their dihedral angles. NMRCORE identified a large LSD, to a great extent corresponding to the A2 and A3 helices and 11 shorter LSDs, each comprising only few residues. We used the largest LSD to fit, in a pairwise manner, all the DBI structures by means of NMRCLUST. The RMS distances, upon fitting, were measured taking into account all the heavy atoms as clustering set. Following this procedure, on the basis of a penalty function [40], NMRCLUST found five clusters, ultimately resulting in five representative structures.

Molecular dynamics (MD) simulations, performed in a water matrix [42] by using the GROMACS1.6 software [43, 44], were used to predict energeti-

cally favoured conformations of the five representative structures of DBI, preliminarily solvated and energy minimized by the steepest descent method. The system was run, first, with backbone position restraining on the peptide for 50 ps to allow a further relaxation of the solvent molecules, and subsequently the run was repeated without any constraint. During these MD runs, the temperature and the pressure were kept constant ($T_0 = 310$ °C, coupling time = 0.1 ps; $P_0 = 1$ bar, coupling time = 0.5 ps). The structures were saved for 100 000 steps, the time step for integration of the equations of motion was 0.002 ps (simulation time: 200 ps). The root mean square deviations (RMSD) of the backbone atoms from the NMR coordinates were analysed to give a relative estimate of the stability. Its value, in a stable protein, fluctuates slightly around an equilibrium value. The RMSD of the backbone atoms, calculated by fitting their positions in each conformation to their NMR coordinates, increases by about 0.2 nm in the first 50 ps of the simulation (Figure 2), and it fluctuates around an equilibrium value during the last 150 ps, when the protein becomes stable.

By using the ANALYSIS module of INSIGHTII [45] (BIOSYM), the atomic average conformation over the set of conformers sampled in the last 150 ps of the simulation was determined. Since the atom averaging can introduce some distortions, the solvated average conformations were subsequently energy minimized with the conjugate gradient algorithm in IN-
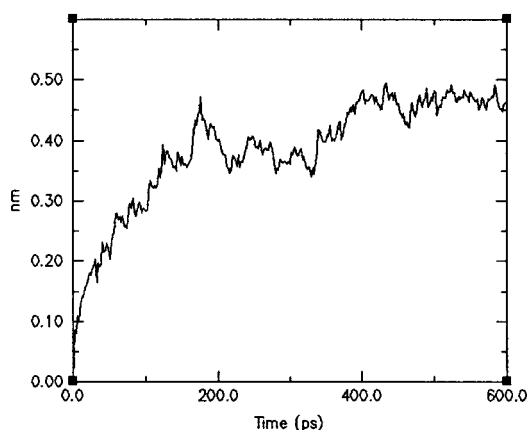
Figure 3. RMSD of all the TTN backbone atoms from the corresponding portion in DBI (see text).
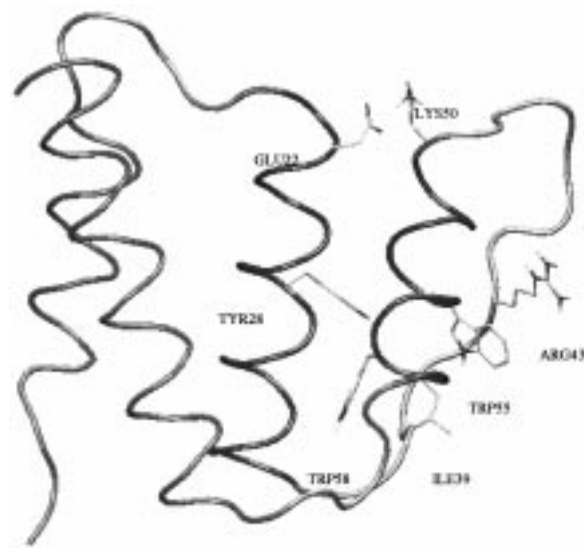

Figure 4. Peptide backbone of the representative structure of DBI. The critical residues for the folding of the flexible region are explicitly displayed.

SIGHTII (conv. crit. = 0.01 kcal/molÅ, dielectric constant = 10).

A further cluster analysis was carried out over the set of five average minimized structures. Two conformationally related subfamilies, consisting of three and two members, were found on the basis of a penalty function [40]. The representative structure of the largest cluster was chosen for further investigations.

Since the sequence 17–50 of the DBI, the tetracontatetraneuropeptide (TTN), bears the main structural features responsible for high affinity to PBR [26, 46], our modeling study was extended also to this peptide. In contrast to DBI, the fragment 17–50 was capable

of displacing [3H] PK11195 from the astrocyte mitochondria, but not [3H]-Flumazenil from the GABA$_A$ extracellular domain, so that it acts as a selective ligand for PBRs [25] (Table 4).

No NMR and X-ray coordinates are available for TTN and therefore the model was built considering the NMR data of DBI. Molecular Dynamics simulations of the TTN model were performed to study, in particular, the stability of the TTN fold.

The structure solvated in a cubic box of SPC water [42] was preliminarily energy minimized, and subsequently MD simulations were performed for 600 ps (the structures were saved for 300 000 steps, the time step for integration of the equations of motion was set to 0.002 ps). The distance between Lys50 and Glu22 was restrained during the simulation. This ionic interaction occurring intermittently with that between Lys50 and Asp21 during the MD simulation of DBI seems to play a crucial role for the folding of active peptides, especially with regard to the conformation of the flexible region. This hypothesis arises from a SAR study of a set of synthetic and natural peptides, which highlights that both polar residues are always present in the active fragments, and the lack of even one of them leads to inactive peptides [26] (Table 5).

The stability of the peptide was monitored by analysing the RMSD of the backbone atoms during the simulation its value fluctuates around a constant value after 380 ps (Figure 3).

The average conformation over the set of conformers sampled in the last 220 ps of the simulation, was subsequently energy minimized, to remove distortion by means of the conjugate gradient algorithm in INSIGHTII (conv. crit. = 0.01 kcal/molÅ, dielectric constant = 10).

A comparison between the DBI and TTN tertiary structures showed a marked difference between the folding of the loop regions. In fact, a more careful examination disclosed that lipophilic interactions between Trp55, Trp58 (both placed in the A3 helix) and Ile39 (placed in the flexible region) may play a key role in determining the DBI loop conformation, as well as the likely edge-to-face aromatic-aromatic interactions [47, 48] between Trp58 (in the A3 helix) and Tyr28 (in the A2 helix), the charge transfer interaction between Trp55 (in the A3 helix) and Arg43 (in the loop region) and the salt bridge formation between Glu22 and Lys50 (Figure 4).

From the alignment of fourteen DBI sequences (Figure 5), coming from several species (by using BLAST in SWISSPROT, S threshold set equal to 100),

Figure 5. Sequence alignment (BLAST) of fourteen DBI peptides from different species.

it can be observed that most of the residues mentioned above are fully conserved. In view of the mentioned interactions, it is conceivable that the conservation of Trp58 is closely linked to that of Tyr28, while the conservation of Trp55 could be linked to that of two other residues, Ile39 and Arg43.

On the basis of these observations, it can be inferred that the role of the A3 helix is of considerable importance for the stabilization of the tertiary structure of DBI, and the different folding of the loop region of TTN may be caused by the lack of this structural motif. However, in TTN, new interactions are detected between the α-helix portion (corresponding to the A2 helix of DBI) and the loop region (Figure 6), now in close contact. Thus, the main chain-main chain hydrogen bond (HB) occurring between Lys16 and Gly21 and the side chain-main chain HB between Thr25 and Leu9, the lipophilic interaction between Tyr12 and Ile23 and the salt bridge occurring between Glu6, Lys34 and Arg27 are the new structural determinants for the folding of the flexible region in TTN.

Results and discussion

3D QSAR investigation

A three-dimensional quantitative structure-activity relationship [32] study was carried out on the molecules listed in Tables 1–3, and aligned following the criteria mentioned before, using molecular fields generated by the GRID16 [49] program.

Since GRID calculates the sum of the interaction energies, but not the separated contributions, and each different probe can bear information about several kinds of interaction [49], more than one probe is typically necessary for a complete description of the interaction model. Hence, we chose Na$^+$, OH$^-$,
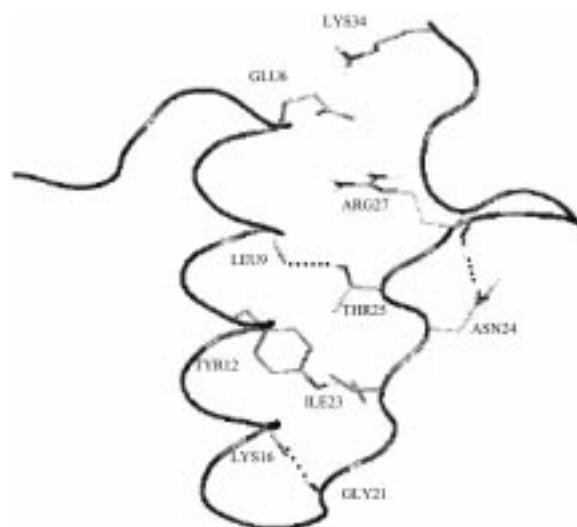

Figure 6. Peptide backbone of TTN. The critical residues for the folding of the flexible region are explicitly displayed.

DRY and C.sp3 (C3) probes to detect electrostatic, HB, lipophilic and Lennard-Jones interactions, respectively.

As usual, a 3D QSAR approach relies on statistical methods to correlate the dependent variable (usually biological activity) with 3D molecular descriptors as the molecular interaction fields of GRID. Instead of a classical PLS method, we used, in combination, different options that GOLPE4.0 [50] offers for the variable pretreatment, to suit the data best. The energies calculated using GRID probes constitute the matrix data of 130 rows (each row represents one ligand) and 21217 columns (each column corresponds to a variable computed at a given grid point).

The repulsive interactions (positive) greater than 5 kcal were truncated to make the overall data distribution more symmetric (*Max cutoff option*), the energy values between −0.01 and 0.05 kcal/mol were set

Table 6. Statistical results from the GRID/GOLPE analysis performed by using DRY, OH$^-$, C.sp3 (C3) and Na$^+$ probes

Var. Selection	Probe	Variables	NOC[a]	r^{2} [b]	Q^{2} [c]	SDEP[d]
PLS	DRY	6918	6	0.890	0.649	0.79
D-optimal design	DRY	1670	6	0.886	0.661	0.78
SRD-FFD	DRY	712	6	0.898	0.761	0.66
PLS	OH$^-$	7064	6	0.866	0.604	0.85
D-optimal design	OH$^-$	1766	6	0.861	0.627	0.82
SRD-FFD	OH$^-$	665	6	0.860	0.721	0.71
PLS	C3	7298	6	0.852	0.594	0.86
D-optimal design	C3	1824	6	0.847	0.617	0.83
SRD-FFD	C3	724	6	0.860	0.721	0.71
PLS	Na$^+$	21043	6	0.874	0.643	0.80
D-optimal design	Na$^+$	1315	6	0.867	0.656	0.79
SRD-FFD	Na$^+$	553	6	0.881	0.744	0.68

[a]Number of optimal components.
[b]Correlation coefficient.
[c]Cross-validated correlation coefficient.
[d]Standard deviation of errors of prediction.

to zero (*Zeroing values option*), the variables with a low standard deviation were set to inactive variables (*Minimum SD option*), and the variables with skewed distribution (2, 3 and 4 level) were deleted (*N-Level option*). Subsequently the D-optimal [51–52] design was repeated many times before the Q^2 started to decrease. The Smart Region Definition (SRD [53, 54]) in combination with Fractional Factorial Design (FFD [55]) was also used to improve the variables selection. The SRD procedure extracts from the matrix of descriptors, groups of neighboring variables, the so-called regions, bearing the same information. The spatial relationship of the variables is not lost and typically the interpretability of the model is increased. The regions generated by SRD was used to improve the variable selection in the FFD selection procedure (no. of seeds = 1/4 no. of variables, critical distance cutoff = 1 Å, collapsing distance cutoff = 2 Å). In Table 6, the statistical results obtained by the application of SRD/GOLPE in comparison with those obtained by a classical PLS [56] analysis are presented.

The best modeling power was achieved with the GRID lipophilic probe DRY, for which six components were sufficient to explain most of the variance of data (r^2 = 0.898) and to give a highly predictive model [57] (Q^2 = 0.761). In order to increase the interpretability of the PLS model, the PLS coefficients (from the sixth component) were plotted as contour plots connecting grid points with similar values. For

instance, a substituent able to engage lipophilic interactions produces a negative DRY field (attractive interactions leading to negative interaction energies), and will be placed in regions with positive PLS coefficients (green polyhedra), if it improves the binding, but in regions with negative PLS coefficients (red polyhedra), if it decreases the affinity.

In Figure 7, some compounds which can help interpreting the model are displayed. Figure 7 reveals that close to position 1 of the arylpyrrolobenzothiazepine **54**, there is no space for substituents, thus the occupation of this space by even a methyl substituent produces unfavourable effects on binding. The amide nitrogen of compound **40** bears a bulky substituent, whose interaction with the probe is also unfavourable for binding. The green areas in Figure 7 indicate the regions where lipophilic interactions enhance binding affinity. In fact, on the amide nitrogen atom of compounds **81**, **101** and **113** lipophilic substituents favour the receptor binding. It is worthy to note that green and red polyhedra occupy regions where additional lipophilic interactions may take place. This could be due to the presence of a region of limited accessibility, where substituents of small size can be accommodated, but where repulsive interactions can occur as the substituent size increases. In addition, halogen atoms, especially the chloro substituent of arylpyrrolobenzoxazepine (**81**) and isoquinoline derivatives (**113**), enhance the receptor affinity, as
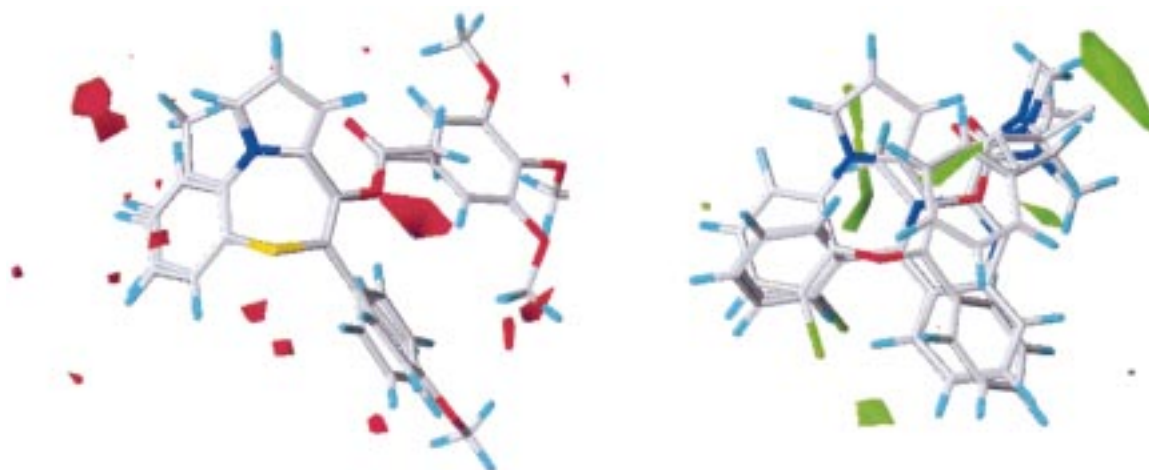
Figure 7. Non cross-validated GRID/GOLPE contour plots (lipophilic DRY probe). Red contours represent regions of interaction decreasing binding affinity. Molecules shown to help interpretation are: **54** (pIC$_{50}$ = 5.30); **40** (pIC$_{50}$ = 4.00) (contour level –0.13). Green contours represent regions of interaction enhancing binding affinity. Molecules shown to help interpretation: **113** (pIC$_{50}$ = 8.70); **81** (pIC$_{50}$ = 8.89); **101** (pIC$_{50}$ = 8.77) (contour level 0.12).

demonstrated by the presence of an additional green region close to it.

Evaluation of the molecular similarity between endogenous and synthetic ligands

GRID/GOLPE study revealed the importance of several hydrophobic contacts in the interaction model, and therefore the possible existence of similar properties shared by synthetic ligands and endogenous peptides was investigated. For the determination of the critical amino acid residues involved in the receptor binding of the endogenous peptides, the molecular interaction fields, computed by means of the lipophilic DRY probe, were evaluated. GRID detected the most energetically favourable lipophilic fields in proximity of the end loop 41–50 of DBI (the resolution of the grid was set to 1 Å). To gain more detailed insights into the topology of the binding residues, the grid spacing was diminished to 0.3 Å in the region pointed out as the most lipophilic in the previous analysis (Figure 8).

To better locate the amino acid residues essential for an efficient binding to PBR, two high affinity compounds, **101** and **81**, were used as templates in a manual superposition aimed to find out whether the main chemical features of these ligands could be mimicked by some amino acids in the sequence where the DRY probe revealed the most favourable interactions. Actually, in the best superposition, the side chains of Phe49, Leu47 and Met 46 could be superposed to the L1, L3 and L4 regions of the synthetic ligands, respec-

Figure 8. Trace of DBI showing energetically favourable interaction fields detected by the lipophilic DRY probe in GRID, in the loop region.
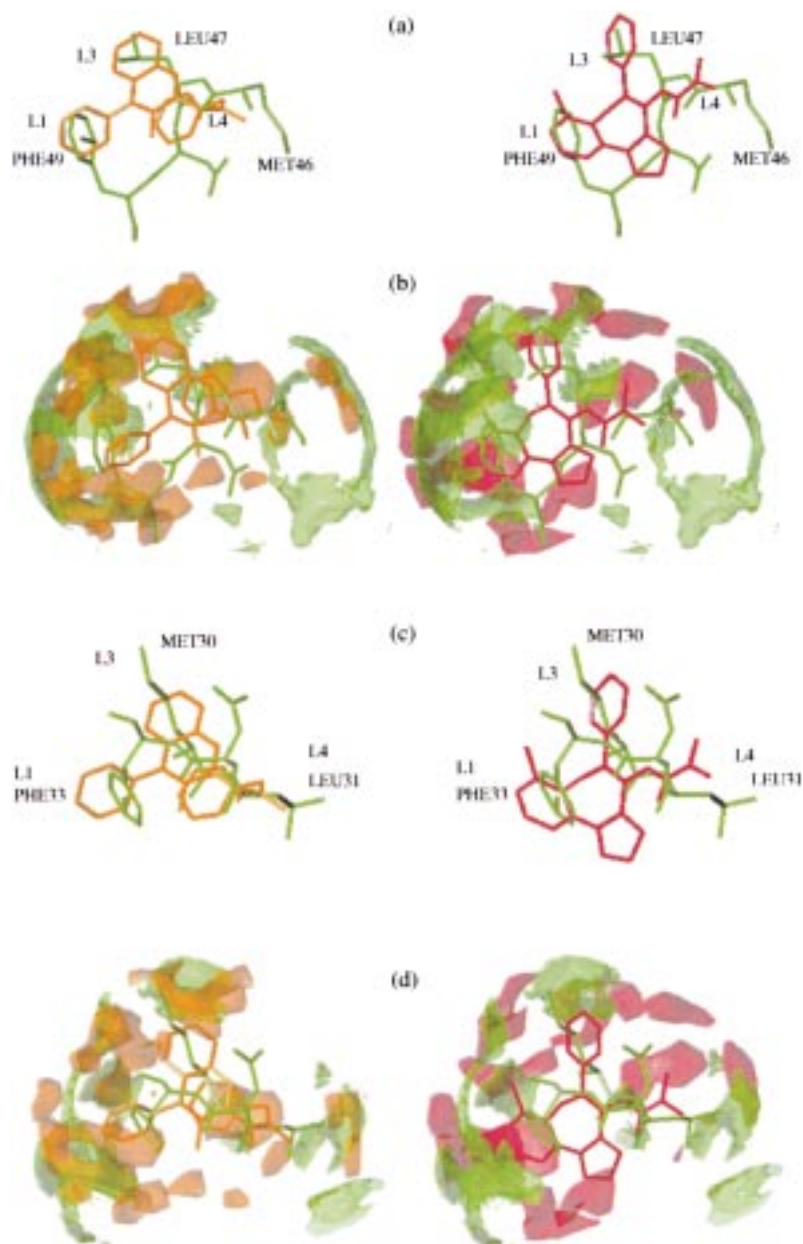
Figure 9. (a) Overlay of critical residues of DBI and two high affinity PBR ligands, **101** (orange, left) and **81** (red, right). (b) GRID interaction fields (green contour at −0.75 kcal/mol; DRY lipophilic probe) of DBI and activity contributions of overlayed ligands **101** (left), **81** (right). (c) Overlay of critical residues of TTN and two high affinity PBR ligands, **101** (orange, left) and **81** (red, right). (d) GRID interaction fields (green contour at −0.75 kcal/mol; DRY lipophilic probe) of TTN and activity contributions of overlayed ligands **101** (left), **81** (right).

tively. In addition, the carbonyl group of Met46 could be aligned with the carbonyl of the amide moiety of the synthetic ligands (Figure 9a).

In order to quantify and visualize the molecular similarity between synthetic and endogenous ligands in terms of lipophilic potentials, the activity contri-

bution regions of compounds **101** and **81**, derived by means of the DRY probe, were considered. These fields represent the molecular potentials which are most useful in describing the ligand affinity, in the GRID/GOLPE model. The comparison between the GRID fields of DBI and high affinity synthetic ligands
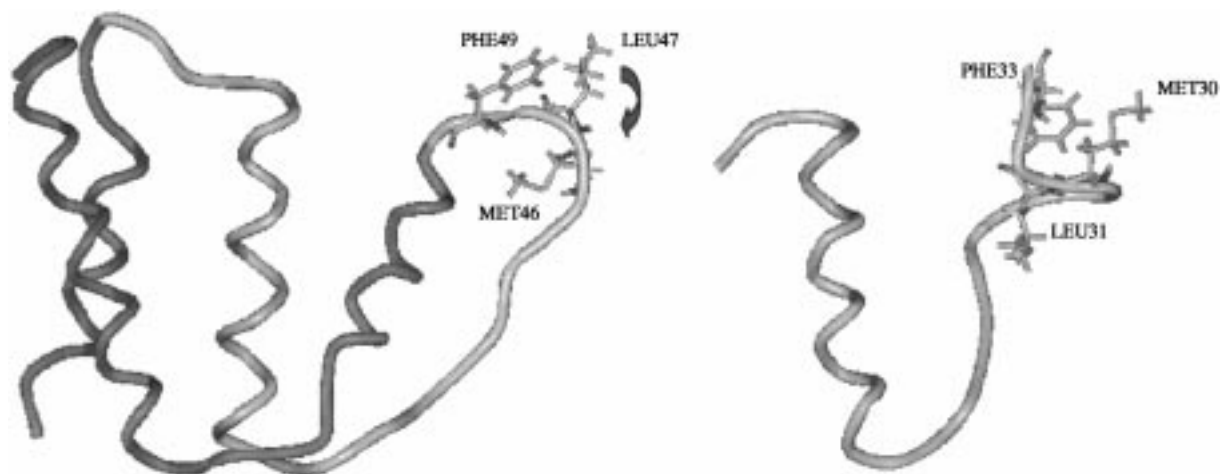
Figure 10. Traces of DBI (left) and TTN (right) highlighting the exchanged spatial positions between methionine and leucine.

revealed a similar distribution of hydrophobic properties (Figure 9b). Therefore it seems that the interaction of endogenous ligands with their binding site is mostly driven by hydrophobic forces, involving the lipophilic side chains of phenylalanine, leucine and methionine. Moreover, an electrostatic interaction, produced by the methionine carbonyl group, could contribute to the intermolecular stabilization of the DBI-PBR complex.

The accessibility to the amino acid residues mentioned before was determined by means of the DSSP [58] software, which computes the number of water molecules in contact with the residues as a criterion to evaluate their solvent exposure. Interestingly, the residues indicated as crucial for the binding at PBRs were found also among the most favoured in terms of solvent accessibility. Moreover, from the alignment of over 10 sequences of DBI from different species it was found that these residues are highly conserved. This could be closely linked to their crucial role in the receptor binding.

Since the shorter fragment of DBI, TTN, still exhibits high affinity toward PBR we tried to find out their similarity in terms of molecular GRID fields. By taking into account the previous findings indicating amino acids Phe48, Leu47 and Met46 as being crucial for the binding of DBI, we examined whether the corresponding residues of TTN were still superimposable onto the two high affinity compounds, **101** and **81**. Indeed, the relative spatial position of Met30 and Leu31 in TTN appears to be inverted if compared with the position of Met46 and Leu47 in DBI (Figure 10), since in this case, the L3 region of the synthetic molecules lies on Met30 and the L4 region on Leu31 (Figure 9c).

However, in Figure 9d, a good degree of similarity can be seen between the TTN lipophilic fields and the activity contribution regions of the two high affinity PBR ligands **101** and **81**.

The negligible effects on molecular similarity observed when the spatial locations of Leu31 and Met30 are interchanged, could also be inferred by analysing the sequence alignments of various DBIs, where it can be appreciated that, although there is no complete exchange between Leu47 and Met46, often leucine can substitute for methionine (Figure 5) in some native DBI sequences.

Recent structure-function relationship studies of proteins indicate that the proline residue can be found in binding site sequences at higher probability than expected by random distribution [59], since, due to the diminished side chain flexibility of this amino acid, it could serve to better maintain the bioactive conformations. In this regard, it was noted that the amino acids of DBI, supposed to interact with the PBR binding site, although belonging to a relatively flexible region, are limited in their mobility by Pro44, on one side, and by the first amino acid of the A3 α-helix (Gly51), on the other side, both acting as geometrical conformational barriers.

By following the hypothesis that complementary electrostatic potentials are essential for a long range recognition [60], we compared the Molecular Electrostatic Potentials (MEPs) of putative interacting sequences of both active endogenous peptides DBI, and TTN with that of two high affinity compounds (**81** and **101**). For this purpose the sequence Phe-Asp-Leu-Met was extracted from TTN and DBI and converted into

the sequence N-Acetyl-Phe-Asp-Leu-NHMe. Since the aspartic acid is not accessible in DBI (the Asp48 accessibility determined by DSSP was only 1/3 of the accessibility of the adjacent residues Phe49 or Leu47), Asp48 was included in a non protonated state to avoid an overestimation of the negative potential. The atomic charges of the truncated fragments and the synthetic molecules were calculated using the 6–31G* ab initio basis set in the SPARTAN software package [61]. As expected, the electrostatic potentials of high activity compounds share common features with those of TTN and DBI (results not shown).

Conclusions and perspectives

In agreement with previous findings coming from the analysis of single classes of PBR ligands, our modeling study, based on a larger and combined array of ligands, lends support to the hypothesis that three structural features, namely two lipophilic regions and one polar group (generally a carbonyl) are essential elements of the PBR interaction model. In addition, the existence of another lipophilic region, significantly modulating the receptor binding, was also confirmed in our investigation.

The comparative molecular field analysis of a high number of PBR ligands showing great molecular diversity and good spread and distribution of binding affinity data, was performed by the GRID/GOLPE methodology using the lipophilic DRY probe. A statistically significant PLS model was formulated, confirming at the 3D level the crucial importance of the lipophilic interactions for efficient receptor binding.

Interactions of a similar nature may be hypothesized also for putative endogenous ligands such as DBI and TTN. Their three-dimensional structures, based on the 3D coordinates of DBI derived from NMR data, showed indeed a common lipophilic region composed by Phe, Leu and Met, easily superimposable to those characterizing the synthetic ligands. In addition, a significant electronic similarity was found comparing the MEPs of synthetic and native PBR ligands.

Overall, our results are consistent with the hypothesis that the receptor binding of both synthetic and endogenous ligands is mainly governed by lipophilic interactions. However, the key role of the lipophilic amino acid triad, Phe, Leu and Met, in PBR binding should be further confirmed through the preparation, by site directed mutagenesis or chemical synthesis, of new DBI and/or TTN derivatives in which the suppos-

edly crucial amino acids are substituted with amino acids bearing non lipophilic side chains.

It is worth noting that our proposed interaction model was established solely on the basis of the molecular features of endogenous and synthetic ligands, as the molecular structure of the binding domain of PK11195 at the PBR is still unknown.

Further characterization of this binding site could be achieved with the development of a pseudoreceptor model which could help to elucidate, at the molecular level, the putative amino acids of the receptor binding site. In addition, useful information could be supplied by site-directed mutagenesis [62] experiments, which could help identifying the key amino acids implicated in the binding of PK11195. Once these data will be available, a more precise description of the topology of the PBR binding site should be possible and this in turn could be particularly helpful for the design of potent and selective PBR ligands.

References

1. Giesen-Crouse, E. (Ed.) Peripheral Benzodiazepine Receptor. Academic Press, London, 1993.
2. McEnery, M.W., Snowman, A.M., Trifiletti, R.R. and Snyder, S.H., Proc. Natl. Acad. Sci. USA, 89 (1992) 3170.
3. Liauzun, E.J., Farges, R., Delmas, P. and Ferrara, P., J. Biol. Chem., 272 (1997) 28102.
4. Wang, J.K.T., Taniguchi, T. and Spector, S., Mol. Pharmacol., 25 (1984) 349.
5. Zisterer, D.M. and Williams, D.C., Gen. Pharmacol., 29 (1997) 305.
6. Mukhin, A.G., Papadopoulos, V., Costa, E. and Krueger, K.E., Proc. Natl. Acad. Sci. U.S.A., 86 (1989) 9813.
7. Papadopoulos, V., Proc. Soc. Exp. Biol. Med., 217 (1998) 130.
8. Papadopoulos, V., Mukhin, A.G., Costa, E. and Krueger, K.E., J. Biol. Chem., 265 (1990) 3772.
9. Black, K.L., Ikezaki, K., Santori, E., Becker, D.P. and Vinters, H.V., Cancer, 65 (1990) 93.
10. Ikezaki, K., Black, K.L., Toga, A.W., Santori, E.M., Becker, D.P. and Smith, M.L., J. Cereb. Blood Flow Metab., 10 (1990) 580.
11. Kapezyk-Subotkowaka, L., Siahaan, T.J., Basile, A., Friedman, H.S., Higgins, P.E., Song, D. and Gallo, J.M., J. Med. Chem., 40 (1997) 1726.
12. Liao, Yi, Kozikowski, A.P., Guidotti, A. and Costa, E., Bioorg. Med. Chem. Lett., 8 (1998) 2099.
13. Schmitt, M., Bourguignon, J.-J., Barlin, G. and Les Davies, B., Aust. J. Chem., 50 (1997) 779.
14. Anzini, M., Cappelli, A., Vomero, S., Giorgi, G., Langer, T., Bruni, G., Romeo, M.R. and Basile, A., J. Med. Chem., 39 (1996) 4275.
15. Campiani, G., Fiorini, I., De Filippis, M., Ciani, S.M., Garofalo, A., Nacci, V., Giorgi, G., Sega, A., Botta, M., Chiarini, A., Budriesi, R., Bruni, G., Romeo, M.R., Manzoni, C. and Mennini, T., J. Med. Chem., 39 (1996) 2922.

16. Trapani, G., Franco, M., Ricciardi, L., Latrofa, A., Genchi, G., Sanna, E., Tuveri, F., Cagetti, E., Biggio, G. and Liso, G., J. Med. Chem., 40 (1997) 3109.

17. Trapani, G., Franco, M., Latrofa, A., Ricciardi, L., Carotti, A., Serra, M., Sanna, E., Biggio, G. and Liso, G., J. Med. Chem., 42 (1999) 3934.

18. Romeo, E., Auta, J., Kozikowski, A.P., Ma, D., Papadopoulos, V., Puia, G., Costa, E. and Guidotti, A., J. Pharm. Exp. Ther., 262 (1992) 971.

19. Okuyama, S., Chaki, S., Yoshikawa, R., Ogawa, S., Suzuki, Y., Okubo, T., Nakazato, A., Nagamine, M. and Tomisawa, K., Life Sci., 64 (1999) 1455.

20. Cappelli, A., Anzini, M., Vomero, S., De Benedetti, P.G., Menziani, M.C., Giorgi, G. and Manzoni, C., J. Med. Chem., 40 (1997) 2910.

21. Kozikowski, A.P., Kotoula, M., Ma, D., Boujrad, N., Tuckmantel, W. and Papadopoulos, V., J. Med. Chem., 40 (1997) 2435.

22. Raghavendra Rao, V.L. and Butterworth, R.F., Eur. J. Pharmacol., 340 (1997) 89.

23. Farges, R., Liauzun, E.J., Shire, D., Caput, D., Le Fur, G., Loison, G. and Ferrara, P., FEBS Lett., 335 (1993) 305.

24. Costa, E. and Guidotti, A., Life Sci., 49 (1991) 325.

25. Barbaccia, M.L., Costa, E. and Guidotti, A., Ann. Rev. Pharmacol. Toxicol., 28 (1988) 451.

26. Bercovich, A., Mcphie, P., Campagnone, M., Guidotti, A. and Hensley, P., Mol. Pharmacol., 37 (1989) 164.

27. Fiorini, I., Nacci, V., Ciani, S.M., Garofalo, A., Campiani, G., Savini, L., Novellino, E., Greco, G., Bernasconi, P. and Mennini, T., J. Med. Chem., 37 (1994) 1427.

28. Campiani, G., Nacci, V., Fiorini, I., De Filippis, M.P., Garofalo, A., Ciani, S.M., Greco, G., Novellino, E., Manzoni, C. and Mennini, T., J. Med. Chem., 32 (1997) 241.

29. Campiani, G., Nacci, V., Fiorini, I., De Filippis, M.P., Garofalo, A., Ciani, S.M., Greco, G., Novellino, E., Williams, D.C., Zisterer, D.M., Woods, M.J., Mihai, C., Manzoni, C. and Mennini, T., J. Med. Chem., 39 (1996) 3435.

30. Dalpiaz, A., Bertolasi, V., Borea, P.A., Nacci, V., Fiorini, I., Campiani, G., Mennini, T., Manzoni, C., Novellino, E. and Greco, G., J. Med. Chem., 38 (1995) 4730.

31. Greco, G., Novellino, E., Fiorini, I., Nacci, V., Campiani, G., Ciani, S.M., Garofalo, A., Bernasconi, P. and Mennini, T., J. Med. Chem., 37 (1994) 4100.

32. Cramer, R.D., Patterson, D.E. and Bunce, J.D., J. Am. Chem. Soc., 110 (1988) 5959.

33. Allen, F.H., Bellard, S., Brice, M.D., Cartwright, B.A., Doubleday, A., Higgs, H., Hummelink, T., Hummelink-Peters, B.G., Kennard, O., Motherwell, W.D.S., Rodgers, J.R. and Watson, D.G., Acta Crystallogr., B35 (1979) 2331.

34. TRIPOS Assoc., St. Louis, MO, U.S.A.

35. Vinter, J.G., Davis, A. and Saunder, M.R., J. Comput.-Aided Mol. Design, 1 (1987) 31.

36. Olson, C. and Christoffersen, R.E. (Eds) Computer Assisted Drug Design, American Chemical Society Symposium 112, Washington, DC, 1979.

37. Mikkelsen, J., Hojrup, P., Nielsen, P.F., Roepstorff, P. and Knudsen, J., Biochem. J., 245 (1987) 857.

38. Swinnen, J.V., Alen, P., Heyns, W. and Verhoeven, G., J. Biol. Chem., 273 (1998) 19938.

39. Andersen, K.V. and Poulsen, F.M., J. Mol. Biol., 226 (1992) 1131.

40. Kelley, L.A., Gardner, S.P. and Sutcliffe, M.J., Protein Eng., 9 (1996) 1063.

41. Kelley, L.A., Gardner, S.P. and Sutcliffe, M.J., Protein Eng., 10 (1997) 737.

42. Pullman, B. (Ed.) Intermolecular Forces, Proceedings of the Fourteenth Jerusalem Symposium on Quantum Chemistry and Biochemistry, D. Reidel Publ. Co., Dordrecht, 1981.

43. van der Spoel, D., van Buuren, A.R., Apol, E., Meulenhoff, P.J., Tielemann, D.P., Sijbers, A.L.T.M., van Drunen, R. and Berendsen, H.J.C., GROMACS manual, Bioson Research Institute and Laboratory of Biophysical Chemistry, University of Groningen, The Netherlands, 1996.

44. van Gunsteren, W.F. and Berendsen, H.J.C., Angew. Chem. Int. Ed. Engl., 29 (1990) 992.

45. Biosym Technologies Inc., San Diego, CA.

46. Slobodyansky, E., Guidotti, A., Wambebe, C., Berkovich, A. and Costa, E., J. Neurochem., 53 (1989) 1276.

47. Burley, S.K. and Pesko, G.A., Science, 229 (1985) 23.

48. Nishio, M., Umezawa, Y., Hirota, M. and Tekeuchi, Y., Tetrahedron, 51 (1995) 8665.

49. Goodford, P.J., J. Med. Chem., 28 (1985) 849.

50. Multivariate Infometric Analysis, Perugia, Italy.

51. Mitchell, T.J., Technometrics, 16 (1974) 203.

52. Steinberg, D.M. and Hunter, W.G., Technometrics, 26 (1984) 71.

53. Kubinyi, H., Folkers, C. and Martin, Y.C. (Eds), 3D QSAR in Drug Design, Recent Advances, Kluwer/ESCOM, Dordrecht, The Netherlands, 1998.

54. Pastor, M., Cruciani, G. and Clementi, S., J. Med. Chem., 40 (1997) 1455.

55. Baroni, M., Costantino, G., Cruciani, G., Riganelli, D., Valigi, R. and Clementi, S., Quant. Struct.-Act. Relat., 12 (1993) 9.

56. Dunn, D.J., Wold, S., Edlund, U. and Helberg, S., Quant. Struct.-Act. Relat., 3 (1984) 131.

57. Cramer, R.D., Bunce, J.D. and Patterson, D.E., Quant. Struct.-Act. Relat., 7 (1988) 18.

58. Kabsch, W. and Sander, C., Biopolymers, 22 (1983) 2577.

59. Herbert, R. and Evans, J., FEBS Lett., 385 (1996) 81.

60. Mannold, R., Kubinyi, H. and Timmerman, H. (Eds) Molecular Modelling-Basic Principles and Applications, VCH Publisher, Inc., New York, NY, 1996.

61. SPARTAN 3.0, Wavefunction, Inc., Irvine, USA.

62. Farges, R., Joseph-Liauzun, E., Shire, D., Caput, D., Le Fur, G. and Ferrara, P., Mol. Pharmacol., 46 (1994) 1160.